Structures, Stabilities, and Ionization Potentials of Dodecahedrane Endohedral Complexes

Damian Moran,[†] Frank Stahl,[†,‡] Eluvathingal D. Jemmis,[§] Henry F. Schaefer III,[†] and Paul von R. Schleyer[†,‡,*]

Center for Computational Quantum Chemistry, University of Georgia, Athens, Georgia 30602, School of Chemistry, University of Hyderabad, Hyderabad 500046, India, and the Computer Chemistry Center, Institut für Organische Chemie der Universität Erlangen-Nürnberg, Henkestr. 42, D-91054 Erlangen, Germany

Received: December 10, 2001; In Final Form: February 13, 2002

The equilibrium geometries and frequencies of endohedral complexes between H, He, Ne, Ar, Li, Li^+, Be, Be^+, Be^{2+}, Na, Na^+, Mg, Mg^+, and Mg^{2+} and dodecahedrane ($X@C_{20}H_{20}$) were computed at B3LYP/6-311+G(d,p). The majority have I_h minima; the exceptions, $X@C_{20}H_{20}$ (X = Be, Be^+, Be^{2+}), have C_{5v} symmetry with X localized against an inner cage face. Cage C−C bonds shorten slightly (<0.01 Å) and cage C−H bonds lengthen slightly (≤0.02 Å) in the series: $M^{2+}@C_{20}H_{20} \rightarrow M^+@C_{20}H_{20} \rightarrow M@C_{20}H_{20}$ (M = Li, Na, Be, Mg). These subtle changes in dodecahedrane geometry are due to donation of electron density from the encapsulated metal atom into the C−C bonding and C−H antibonding endohedral complex HOMO, which has a structure closely resembling the LUMO (A_{1g}) of dodecahedrane. The zero point-corrected inclusion energies of $Li^+@C_{20}H_{20}$ (I_h; −12.7 kcal/mol), $Be^+@C_{20}H_{20}$ (C_{5v}; −1.3 kcal/mol), $Be^{2+}@C_{20}H_{20}$ (C_{5v}; −236.3 kcal/mol) and $Mg^{2+}@C_{20}H_{20}$ (I_h; −118.0 kcal/mol) are exothermic relative to their isolated components. However, all the endohedral dodecahedrane complexes are higher in energy than their corresponding exohedral isomers. Endohedral He and Li^+ chemical shifts are 0.9 and 1.9 ppm, respectively. $M@C_{20}H_{20}$ (M = Li, Na, Be, Mg) species possess lower first ionization potentials than the Cs atom (3.9 eV) and, therefore, are "superalkalis". Removal of dodecahedrane hydrogens can increase endohedral complex stability significantly. Thus, endohedral beryllium in the beryllocene complex, $Be@C_{20}H_{10}$ (D_{5d}) is 75.3 kcal/mol more stable than its isolated components, in contrast with $Be@C_{20}H_{20}$ which is unstable by 127.7 kcal/mol. Dodecahedrane, $He@C_{20}H_{20}$ and $Li^+@C_{20}H_{20}$ B3LYP/6-31G(d) and B3LYP/6-311+G(d,p) absolute energies did not change significantly (<0.31 kcal/mol) when computed using either a pruned (75,302) or pruned (99,590) integration grid; with the addition of zero point energy the maximum deviation was less than 0.53 kcal/mol.

Introduction

Many members of a new class of novel materials,[1,2] endohedral fullerene complexes incorporating metal cations,[3,4] noble gas,[5,6] and nitrogen atoms,[7,8] have been prepared. However, until very recently endohedral complexes of smaller hydrocarbon cages such as dodecahedrane (Figure 1) have largely been relegated to the realm of computation (vide infra). Dodecahedrane has an interior diameter of 4.4 Å, 40% smaller than the 7.1 Å diameter of C_{60}. Since only low degrees of incorporation have been achieved experimentally in forcing atoms such as He (0.02% $He@C_{60}$)[9] inside fullerenes, the prospects for synthesizing an endohedral derivatized dodecahedrane molecule appeared poor. Recently, however, Cross, Saunders, and Prinzbach[10] applied their helium molecular beam bombardment procedure (developed for $X@C_{60}$) to $C_{20}H_{20}$ and obtained ≥200 μg of $He@C_{20}H_{20}$. The degree of He incorporation (0.01% $He@C_{20}H_{20}$) was comparable to that resulting from helium bombardment of C_{60}.

In 1978, Schulman and Disch[11] used INDO and CNDO methods to study dodecahedrane, its fluorinated derivatives, and the inclusion compounds, $X@C_{20}H_{20}$ (X = e^-, H, H^+, H^-, Li^+, Be, Na^+, and H_2).[12] The latter were evaluated by comparing the energy of $X@C_{20}H_{20}$ with the sum of the energies of the components; we refer to this quantity as the inclusion energy, E_{inc} (kcal/mol) shown in Table 1. The levels of theory at the time were insufficient to estimate accurate inclusion energies. However, they did conclude that the radical anion of dodecahedrane was unstable (by 149 kcal/mol) because the additional electron had to occupy a strongly antibonding orbital (Figure 2). Subsequent computational studies of endohedral dodecahedrane derivatives (Table 1) include Dixon, Deerfield and Graham's[13] PRDDO $X@C_{20}H_{20}$ (X = H^+, H_2, He, Li^+, Li^-, Be, and Be^{2+}) analysis, Disch and Schulman's[14] HF/STO-3G $X@C_{20}H_{20}$ (X = H^+, He, Li^+, Be, Be^+, Be^{2+}, Na^+, and Mg^{2+}) investigation, and the recent report from Jimenez-Vazquez, Tamariz and Cross[15] on higher level B3LYP and MP2 calculations on $He@C_{20}H_{20}$ and $Ne@C_{20}H_{20}$.

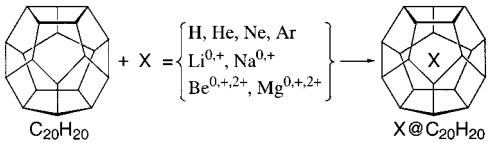

Figure 1. Endohedral dodecahedrane derivatives, $X@C_{20}H_{20}$.

Dixon et al.[13] reported exothermic inclusion energies for $H^+@C_{20}H_{20}$ and $Be^{2+}@C_{20}H_{20}$, which they attributed to the small sizes of the encapsulated ions and polarization stabilization between the charged particle and the hydrocarbon cage. Disch and Schulman[14] computed exothermic inclusion energies for

* Corresponding author. E-mail: schleyer@chem.uga.edu.
† University of Georgia.
‡ Universität Erlangen-Nürnberg.
§ University of Hyderabad.

10.1021/jp014471z CCC: $22.00
Published on Web 04/18/2002

TABLE 1: Summary of Computed Inclusion Energies (E_{inc}), Evaluated as the Difference between the Absolute Energy of $X@C_{20}H_{20}$ and the Sum of the Separated Components (kcal/mol) (X is the encapsulated species, located at the mid-point of each cage)

$X@C_{20}H_{20}$	H	He	Ne	Li^+	Li	Li^-	Na	Na^+	Be	Be^+	Be^{2+}	Mg	Mg^{2+}
INDO/CNDO[a,11]	−30	22		−183[d]	25			420[d]	−519				
PRDDO[b,13]		45.7		15.4		304.4			307.6		−112.6		
HF/STO-3G[c,14]		43.3		−5.2				76	299	107	−167		−56.7
B3LYP/6-311G(d,p)[e,15]		37.5	100.7										
MP2/6-311G(d,p)[f,15]		33.8	98.3										
radius (Å)[45]	0.12	0.12	0.234	0.06	0.13		0.154	0.095	0.125		0.031	0.145	0.065

[a] $r_{cc} = 1.54$ Å, and $r_{CH} = 1.09$ Å. [b] $r_{C-C} = 1.53$ Å, and $r_{CH} = 1.10$ Å. [c] $r_{C-C} = 1.54$ Å, and $r_{CH} = 1.09$ Å. [d] This is a CNDO/2 value. [e] B3LYP/6-311G(d,p) geometry plus B3LYP/6-311G(d,p) ZPE correction. [f] MP2/6-311G(d,p) geometry plus B3LYP/6-311G(d,p) ZPE and counterpoise correction.

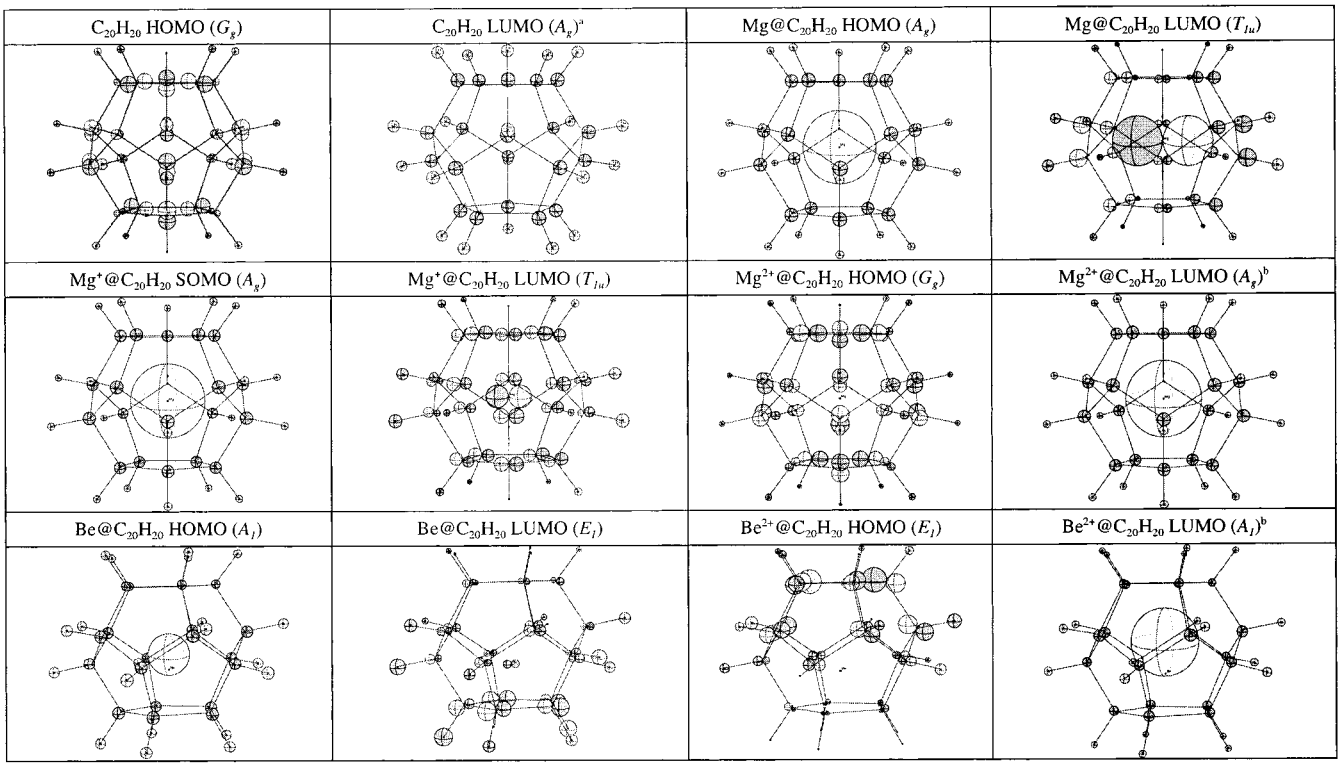

Figure 2. $C_{20}H_{20}$ (I_h), $Mg^{0,+,2+}@C_{20}H_{20}$ (I_h) and $Be^{0,2+}@C_{20}H_{20}$ (C_{5v}) frontier molecular orbitals. Note the C−C bonding and C−H antibonding contributions to the HOMO of $Mg@C_{20}H_{20}$ and $Be@C_{20}H_{20}$, the SOMO of $Mg^+@C_{20}H_{20}$, and the LUMO of $C_{20}H_{20}$, $Mg^{2+}@C_{20}H_{20}$ and $Be^{2+}@C_{20}H_{20}$.

$X@C_{20}H_{20}$ (X = H^+, Li^+, Be^{2+} (^1A_g) and Mg^{2+}) at the HF/STO-3G level with $Be^{2+}@C_{20}H_{20}$ best (−167 kcal/mol). E_{inc} $He@C_{20}H_{20}$ was moderately endothermic (43 kcal/mol) while $Be@C_{20}H_{20}$ was the least stable (299 kcal/mol relative to uncomplexed Be and dodecahedrane). Disch and Schulman[14] found that the atomic charges on Li^+ (+0.96) and Na^+ (+0.96) were close to unity and noted that the extent of covalent interaction between the cage and Li^+ and Na^+ was negligible, e.g., Li^+ 2s 0.01 e, 2p 0.12 e at the HF/STO-3G level. The $Be^{2+}@C_{20}H_{20}$ endohedral derivative, however, did show considerable charge transfer from the cage framework (0.94 e) into the beryllium 2s and 2p orbitals leading to an approximate sp^3 hybridization ratio. Finally, Disch and Schulman[14] estimated that the electron affinity of $Be^{2+}@C_{20}H_{20}$ was 138.5 kcal/mol, close to that of unencapsulated Be^+ (156.9 kcal/mol) but much less than unencapsulated Be^{2+} (407.9 kcal/mol). Therefore, they concluded that the difference in electron affinity between $Be^{2+}@C_{20}H_{20}$ and unencapsulated Be^{2+} arose as in the former the beryllium was in charge state +1, with nearly one electron transferred from the framework, in strong agreement with their computed beryllium atomic charge of +1.

Jimenez-Vazquez et al.[15] computed B3LYP/6-311G(d,p) + zero point energy (ZPE) He and Ne inclusion energies of 37.5 and 100.7 kcal/mol, respectively (Table 1). The E_{inc}, however, decreased around 3 kcal/mol at MP2/6-311G(d,p)//MP2/6-311G(d,p) + B3LYP/6-311G(d,p) ZPE to 33.8 kcal/mol ($He@C_{20}H_{20}$) and 98.3 kcal/mol ($Ne@C_{20}H_{20}$). They noted that the dodecahedrane cage distorted very little after the introduction of He or Ne, and that there was a small (~3 kcal/mol) change in zero point energy after encapsulation resulting from a new T_{1u} vibration in the endohedral complex. Jimenez-Vazquez et al.[15] also compared the GIAO/B3LYP/6-311+G(3df,2p) He NMR chemical shift relative to the unencapsulated noble gas and found that the endohedral helium atom was slightly deshielded by 1.51 ppm.[16]

In light of the recent experimental success of Cross, Saunders, and Prinzbach,[10] we have extended our previous related studies on endohedral borane, alane, and gallane complexes[17−21] to dodecahedrane inclusion complexes using density functional theory calculations.[22] First, the stabilities of geometry optimized endohedral and exohedral complexes were probed by computing endohedral inclusion energies (E_{inc}) = $X@C_{20}H_{20}$ − [$C_{20}H_{20}$ − X], exohedral binding energies (E_{bind}) = X − $C_{20}H_{20}$ − [$C_{20}H_{20}$ − X] and exo ↔ endo isomerization energies (E_{isom}) = $X@C_{20}H_{20}$ − X − $C_{20}H_{20}$). Second, the energies of geometry optimized endohedral complexes was used to calculate ionization

TABLE 2: Gaussian 94 (G94) and Gaussian 98 (G98), B3LYP/6-31G(d) and B3LYP/6-311+G(d,p) $C_{20}H_{20}$, $He@C_{20}H_{20}$, and $Li^+@C_{20}H_{20}$ Absolute Energy, Zero Point Energy (ZPE, kcal/mol), and First Vibrational Frequency (ω_1) Computed Using (75,302) and (99,590) DFT Intergration Grids with Very Tight SCF Convergence

	B3LYP/6-311+G(d,p)				B3LYP/6-31G(d)			
	G94 (75,302)	G94 (99,590)	G98 (75,302)	G98 (99,590)	G94 (75,302)	G94 (99,590)	G98 (75,302)	G98 (99,590)
$C_{20}H_{20}$								
energy	−774.35923	−774.35967	−774.35951	−774.35963	−774.18505	−774.18548	−774.18538	−774.18548
ZPE	223.89	223.56	224.02	224.06	225.64	225.80	225.76	225.80
ω_1 (cm^{-1})	477.8	474.9	478.5	479.6	479.5	481.8	480.2	481.8
$He@C_{20}H_{20}$								
energy	−777.21667	−777.21665	−777.21647	−777.21658	−777.03629	−777.03641	−777.03626	−777.03641
ZPE	226.81	226.78	226.73	226.76	228.57	228.54	228.49	228.55
ω_1 (cm^{-1})	503.4	503.1	502.4	502.5	505.0	505.4	505.1	505.5
$Li^+@C_{20}H_{20}$								
energy	−781.66671	−781.66666	−781.66622	−781.66631	−781.49796	−781.49806	−781.49791	−781.49806
ZPE	225.10	225.04	225.01	225.03	226.30	226.45	226.40	226.45
ω_1 (cm^{-1})	367.0	367.9	355.8	355.2	330.7	362.7	347.6	363.0

potentials and natural charge analysis used to obtain atomic hybridizations and charges. Third, as first noted by Schulman and Disch,[11] NMR spectroscopy is a powerful tool for detecting $X@C_{20}H_{20}$ and consequently we computed chemical shifts for promising even-electron endohedral derivatives (X = ^{3}He and $^7Li^+$) as an aid to future experimental efforts.[23] Our results, which extend earlier theoretical predictions, highlight the size dependence of endohedral complex stability and reveal the dramatic effect of encapsulation on the ionization potentials of the enclosed atoms. Finally, another way to achieve endohedral binding is to remove dodecahedrane hydrogens and to this end, we explore prototype beryllocene ($Be@C_{20}H_{10}$) and magnesocene ($Mg@C_{20}H_{10}$) structures.

Methods

Patchkovskii and Thiel[24] computed the inclusion energy for $He@C_{60}$ using Turbomole[25,26] and Gaussian 94[27] DFT integration grids ranging in size from 1742 and up to 149 504 grid points per carbon atom. They found that E_{inc} only converged (to within 0.2 kcal/mol) for the larger DFT integration grids, e.g., spherical product (96,32,63) in Gaussian 94[27] and Lobato (95,32,64) in Turbomole.[25,26] As a test, we computed the B3LYP/6-31G(d) and B3LYP/6-311+G(d,p) energy, zero point energy and vibrational frequencies for $C_{20}H_{20}$, $He@C_{20}H_{20}$ and $Li^+@C_{20}H_{20}$ using Gaussian 94's[27] (G94) and Gaussian 98's[22] (G98) pruned (75,302) fine and (99,590) ultrafine grids. From Table 2 it can be seen that for a given basis set, the energies, ZPEs, and first vibrational frequencies are essentially identical and that there is no evidence for a grid effect for either the empty cage or the endohedral complexes. Furthermore, despite the changes introduced into G98[22] to improve the efficiency with which DFT frequencies are computed,[28] the different generations of Gaussian produce very similar results. Therefore, we used the G98[22] default pruned (75,302) fine integration grid to evaluate final B3LYP/6-311+G(d,p) energies, frequencies, and GIAO NMR chemical shifts. We did not examine the effect of grid size on the exohedral complexes, which were computed using the G98[22] default (75,302) fine grid, as were all B3LYP/6-31G(d) results reported herein.

Endohedral complexes, $X@C_{20}H_{20}$ (X = H, He, Ne, Ar, Li, Li^+, Na, Na^+, Be, Be^+, Be^{2+}, Mg, Mg^+, Mg^{2+}) (Figure 1) were B3LYP/6-311+G(d,p)[29] optimized in I_h symmetry using Gaussian 98;[22] frequency analyses (at the same level) characterized the optimized structures. The C_{5v} symmetric endohedral minima, $X@C_{20}H_{20}$ (X = Be, Be^+, Be^{2+}) were computed in the same way. The B3LYP/6-311+G(d,p) wave functions were stable for both the I_h and C_{5v} $Be@C_{20}H_{20}$, $Be^+@C_{20}H_{20}$, and $Be^{2+}@C_{20}H_{20}$ endohedral derivatives.

Exohedral complexes, $X-C_{20}H_{20}$ (X = He, Ne, Li, Li^+, Li^-, Na, Na^+, Be^+, Be^{2+}, Mg^+, Mg^{2+}) also were B3LYP/6-311+G(d,p) optimized in C_{5v} symmetry. B3LYP/6-31G(d) frequencies were computed for the exohedral cation (Li^+, Na^+, Be^+, Mg^+) and dication (Be^{2+}, Mg^{2+}) complexes, optimized at the same level. $X-C_{20}H_{20}$ (X = He, Ne, Li, Li^-, Na, Be, Mg) exohedral binding energies were negligible and frequencies were not meaningful for these weakly interacting complexes.

Decadehydrododecahedrane ($C_{20}H_{10}$) and its metallocene complexes, $M@C_{20}H_{10}$ (M = Be, Mg) were B3LYP/6-31G(d) optimized in D_{5d} symmetry using Gaussian 98;[22] frequency analyses (at the same level) characterized the metal-incorporated structures as minima. $C_{20}H_{10}$ had a UB3LYP/6-31G(d) triplet minimum; optimization as a singlet (same level) failed to converge since the distal cyclopentadienyl radical moieties do not "communicate" electronically.

Atomic charges were provided by Natural Bond Order (NBO) analysis.[30] Geometric parameters, unscaled zero point energies (ZPE), lowest frequencies (ω_1), and natural charges summarized in Tables 3, 4, 5, and 6. B3LYP/6-311+G(d,p) vertical and adiabatic $M@C_{20}H_{20}$ (M = Li^-, Li, Na, Be, Be^+, Mg, Mg^+) ionization potentials given in Table 7.

$He@C_{20}H_{20}$ and $Li^+@C_{20}H_{20}$ B3LYP/6-311+G(d,p) NMR chemical shifts were computed using the Gauge-Independent Atomic Orbital (GIAO) method, as implemented in Gaussian 98.[22] Nucleus Independent Chemical Shifts (NICS)[31,32] were computed GIAO/B3LYP/6-311+G(d,p) at the center of dodecahedrane ($Bq@C_{20}H_{20}$)[33] and a five-membered ring face. Individual contributions of bonds and core electrons to endohedral Bq, He, and Li^+ total shieldings were evaluated using Kutzelnigg's Individual Gauge for Localized Orbitals (IGLO) method,[34] as implemented in the deMon NMR program,[35] in conjunction with the Perdew-Wang-91 functional and IGLO−III TZ2P basis set. Magnetic shieldings and chemical shifts are summarized in Table 8.

Results and Discussion

Geometries. Table 3 contains the optimized bond lengths and lowest vibrational frequencies (or imaginary frequencies) for I_h dodecahedrane, dodecahedrane radical cation, dodecahedrane radical anion, and $X@C_{20}H_{20}$ derivatives. Whereas the dodecahedrane radical anion minimum retains I_h symmetry, icosahedral dodecahedrane radical cation has three imaginary frequencies; Jahn−Teller distortion (shown in Figure 3) leads to a D_{2h} $C_{20}H_{20}^+$ minimum (shown in Figure 4).[36]

TABLE 3: I_h Symmetry Optimized $C_{20}H_{20}$, $C_{20}H_{20}^{+\bullet}$, $C_{20}H_{20}^{-\bullet}$, and $X@C_{20}H_{20}$ B3LYP/6-311+G(d,p) Absolute Energies (H_a), ZPE (kcal/mol), Lowest Vibrational Frequency (cm^{-1}) [or imaginary frequency] and Optimized Bond Lengths (Å) [The $C_{20}H_{20}$ radical cation is a D_{2h} minima (see Figures 3 and 4 for details).]

	energy	ZPE	ω_1	r_{C-X}	r_{C-C}	r_{C-H}
$C_{20}H_{20}$	−774.35963	224.06	479.6	2.179[a]	1.555	1.092
$C_{20}H_{20}^{+\bullet}$	−774.04135[b]	216.10[b]	−330.2*i* (NImag=3)[b]	2.201[a,b]	1.538[b]	1.098[b]
$C_{20}H_{20}^{-\bullet}$	−774.33343	217.30	252.2	2.174[a]	1.552	1.098
$H@C_{20}H_{20}$	−774.80902	226.79	487.3	2.188	1.562	1.093
$He@C_{20}H_{20}$	−777.21658	226.76	502.5	2.190	1.563	1.092
$Ne@C_{20}H_{20}$	−903.15732	224.91	507.5	2.214	1.580	1.091
$Ar@C_{20}H_{20}$	−1301.39582	219.35	615.7	2.274	1.623	1.093
$Li@C_{20}H_{20}$	−781.76771	222.43	513.2	2.196	1.567	1.092
$Li^+@C_{20}H_{20}$	−781.66631	225.01	355.2	2.200	1.570	1.087
$Li^-@C_{20}H_{20}$	−781.78384	222.04	342.0	2.195	1.566	1.094
$Na@C_{20}H_{20}$	−936.45802	222.68	525.9	2.220	1.584	1.091
$Na^+@C_{20}H_{20}$	−936.36031	224.87	446.1	2.223	1.586	1.086
$Be@C_{20}H_{20}$	−788.81668	215.95	356.3*i* (NImag = 3)	2.202	1.571	1.101
$Be^+@C_{20}H_{20}$	−788.67060	218.99	522.2*i* (NImag = 3)	2.205	1.574	1.093
$Be^{2+}@C_{20}H_{20}$	−788.36842	220.77	369.8*i* (NImag = 3)	2.202	1.571	1.087
$Mg@C_{20}H_{20}$	−974.15435	217.23	371.3	2.221	1.585	1.098
$Mg^+@C_{20}H_{20}$	−974.02868	219.35	364.8	2.224	1.587	1.093
$Mg^{2+}@C_{20}H_{20}$	−973.78767	223.40	381.7	2.227	1.589	1.085

[a] In this case, X is a dummy point placed at the center of the cage. [b] B3LYP/6-31G(d) optimized geometry and frequency.

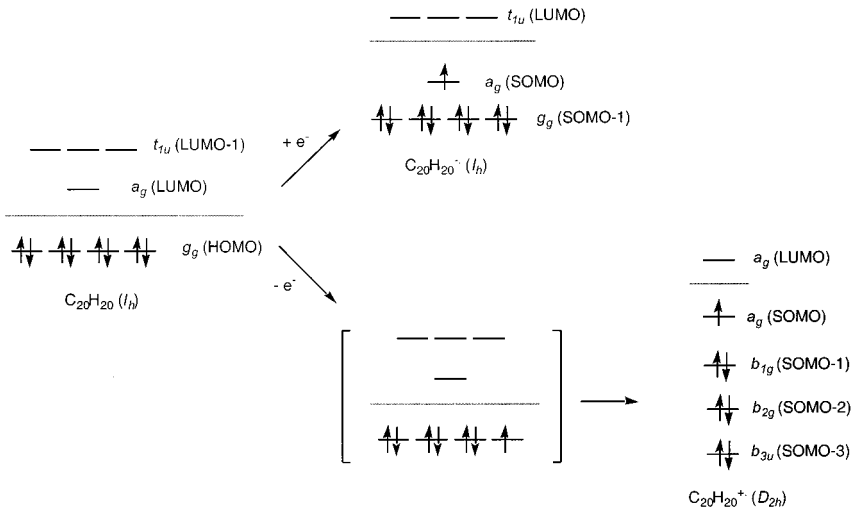

Figure 3. Schematic showing the salient molecular orbitals of dodecahedrane, its radical anion, and radical cation. Note the Jahn−Teller distortion from I_h to D_{2h} by the dodecahedrane radical cation.

With the exception of $Be@C_{20}H_{20}$, $Be^+@C_{20}H_{20}$, and $Be^{2+}@C_{20}H_{20}$, all I_h dodecahedrane inclusion complexes are minima. Following the triply degenerate T_{1u} imaginary frequencies for all three beryllium derivatives results in C_{5v} endohedral complexes (Table 4), with the endohedral atoms located against an inner cage face (shown in Figure 5). The twelve identical minima correspond to a "monkey saddle" of higher order.[37] The Be−C bond distances to the adjacent cage faces are: 1.793 Å ($Be@C_{20}H_{20}$), 1.758 Å ($Be^+@C_{20}H_{20}$), and 1.735 Å ($Be^{2+}@C_{20}H_{20}$). The smallest ion in our set of endohedral units is Be^{2+} and the face localized, C_{5v} minimum maximizes the electrostatic interaction between the dication and the cage. The minimum involving Mg^{2+}, however, has I_h symmetry. Apparently, Mg^{2+} (computed charge +1.69) is too large to fit against a cage face. It is, therefore, somewhat surprising that endohedral beryllium, which has twice the radius of Mg^{2+} (Table 1), has a C_{5v} minimum. This implies that the encapsulated metal has transferred significant electron density onto the hydrocarbon cage, thus reducing its radius sufficiently to allow it to adopt a face localized structure. Indeed, the endohedral beryllium natural charge of +1.25 supports this conclusion.

$Mg@C_{20}H_{20}$ has the longest C−H bond lengths (1.098 Å) of the icosahedral dodecahedrane derivatives, while $Mg^{2+}@C_{20}H_{20}$ has the shortest C−H bonds (1.085 Å). Similarly, it can be seen in Figure 7 that the C−H bonds are longer in $Li@C_{20}H_{20}$ and $Na@C_{20}H_{20}$ than in $Li^+@C_{20}H_{20}$ and $Na^+@C_{20}H_{20}$, respectively. These subtle changes in dodecahedrane geometry upon complex formation can be understood by examining the LUMO of the parent $C_{20}H_{20}$ (shown in Figure 2), which is C−H antibonding and C−C bonding. The odd electron of the radical anion of dodecahedrane occupies this molecular orbital (SOMO) and, therefore, as shown in Figures 7 and 8, the C−C bonds shorten and C−H bonds elongate. Similarly, the LUMO of $M^+@C_{20}H_{20}$ (M = Li, Na) and $M^{2+}@C_{20}H_{20}$ (M = Be, Mg; shown in Figure 2) endohedral complexes are C−H antibonding and C−C bonding. Natural charge analysis (vide infra; Table 5) reveals that metals are significantly ionized when encapsulated. They donate electron density into these $M^+@C_{20}H_{20}$ and $M^{2+}@C_{20}H_{20}$ LUMOs and at the same time reduce their atomic radius, strengthen the cages C−C framework, and lengthen the C−H bonds. Further evidence for this effect comes both from the trend in $X@C_{20}H_{20}$ C−C bond lengths (Figure 8), which are longer in $M^{+/2+}@C_{20}H_{20}$ (M = Li, Na, Be, and Mg) cation and dication complexes than in their corresponding neutral $M@C_{20}H_{20}$ complexes,[38] and from comparison of the bond lengths in dodecahedrane radical anion (C−C = 1.552 Å; C−H = 1.098

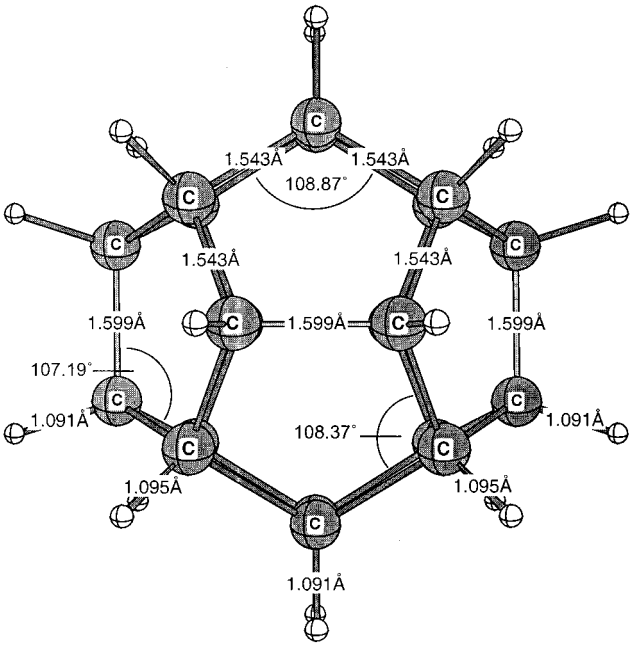

Figure 4. Equilibrium geometry of B3LYP/6-311+G(d,p) optimized D_{2h} dodecahedrane radical cation.

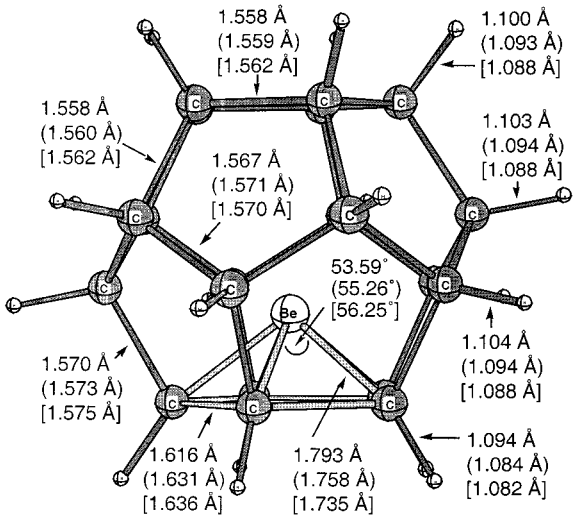

Figure 5. Bond distances and C−Be−C bond angle for C_{5v} endohedral (a) Be@$C_{20}H_{20}$, (b) Be^{+}@$C_{20}H_{20}$ (parenthetic), and (c) Be^{2+}@$C_{20}H_{20}$ [bracketed] B3LYP/6-311+G(d,p) optimized (NImag = 0).

TABLE 4: Non I_h Symmetry Optimized $C_{20}H_{20}$ Radical Cation and Endohedral X@$C_{20}H_{20}$ B3LYP/6-311+G(d,p) Absolute Energies (H_a), ZPE (kcal/mol), Lowest Vibrational Frequency (cm^{-1}) [Or Imaginary Frequency] and Optimized Bond Lengths (Å)

	sym.	energy (H_a)	ZPE	ω_1	geometry
H@$C_{20}H_{20}$ (B3LYP/6-31G(d))	C_{3v}	−774.59594	225.75	638.3	Figure 6
Be@$C_{20}H_{20}$	C_{5v}	−788.82960	218.22	263.7	Figure 5a
Be^{+}@$C_{20}H_{20}$	C_{5v}	−788.69487	222.00	297.3	Figure 5b
Be^{2+}@$C_{20}H_{20}$	C_{5v}	−788.38709	222.81	240.0	Figure 5c
$C_{20}H_{20}^{+\bullet}$	D_{2h}	−774.04236	216.35	173.7	Figure 4

Å) with dodecahedrane (C−C = 1.555 Å; C−H = 1.092 Å). However, the effect of metal, cation, and dication encapsulation on dodecahedrane bond lengths is small—the total distortions in the C−C and C−H bond lengths are less than 0.03 Å. This is expected since the relevant molecular orbital involves all forty atoms in the cage. Therefore, the influence on any one bond is minor.

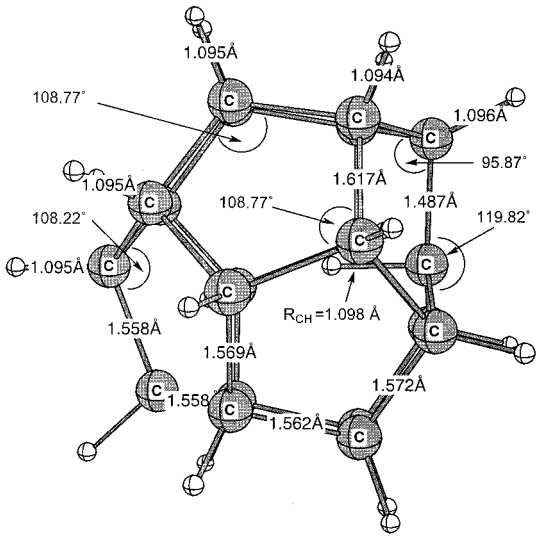

Figure 6. Bond lengths and angle for endohedral H@$C_{20}H_{20}$ UB3LYP/6-31G(d) optimized in C_{3v} symmetry (displaced hydrogen omitted).

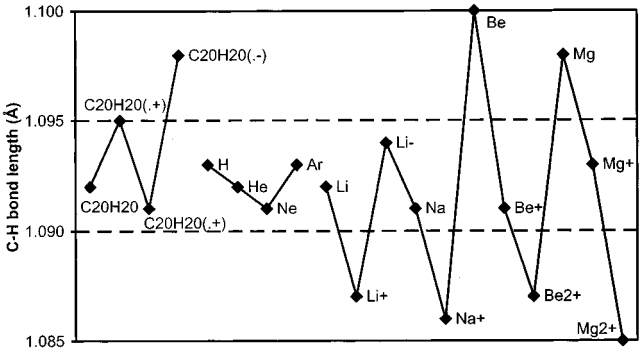

Figure 7. Graph of C−H bond length (Å) trend in X@$C_{20}H_{20}$ endohedral derivatives. Dodecahedrane, its I_h radical anion, and D_{2h} radical cation are included for reference. With the exception of X@$C_{20}H_{20}$ (X = Be, Be^{+}, Be^{2+}), endohedral complex structures were B3LYP/6-311+G(d,p) optimized in I_h symmetry; the former were optimized in C_{5v} and their average C−H bond length (Å) plotted. Note the behavior of neutral Be and Mg, which have an appreciable natural charge.

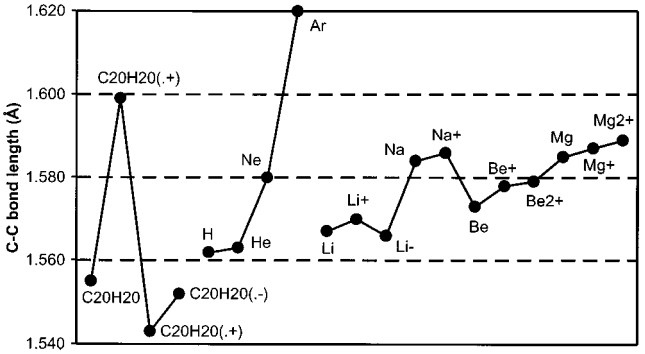

Figure 8. Graph of C−C bond length (Å) trend in X@$C_{20}H_{20}$ endohedral derivatives. Dodecahedrane, its I_h radical anion, and D_{2h} radical cation are included for reference. With the exception of X@$C_{20}H_{20}$ (X = Be, Be^{+}, Be^{2+}), endohedral complex structures were B3LYP/6-311+G(d,p) optimized in I_h symmetry; the former were optimized in C_{5v} and their average C−C bond length (Å) plotted.

There also is a small distortion (ΔC−C ≤ 0.025 Å) in the structure of dodecahedrane following introduction of He and Ne and a mere 0.068 Å stretching of the C−C bonds following encapsulation of the largest species we computed inside $C_{20}H_{20}$, Ar (Table 3). Jimenez-Vazquez et al.[15] reported identical

TABLE 5: B3LYP/6-311+G(d,p) Endohedral Complex Inclusion Energies (E_{inc}; kcal/mol),[a] Natural Charges, and Exohedral and Endohedral Isomerization Energies (E_{isom}; kcal/mol)[b]

	sym.	E_{inc}	q_X	q_C	q_H	q_{C-H}	$\sum q_{C-H}$	E_{isom}
$C_{20}H_{20}$	I_h			−0.25	0.25	0.00	0.00	
$C_{20}H_{20}^{+\bullet}$	D_{2h}			−0.24[c]	0.29[c]	0.05[c]	1.00[c]	
$C_{20}H_{20}^{-\bullet}$	I_h			−0.24	0.19	−0.05	−1.00	
$H@C_{20}H_{20}$	I_h	35.84	0.08	−0.25	0.25	0.00	0.00	
$He@C_{20}H_{20}$	I_h	37.89	0.07	−0.25	0.25	0.00	0.00	35.41
$Ne@C_{20}H_{20}$	I_h	102.96	0.09	−0.25	0.25	0.00	0.00	102.45
$Ar@C_{20}H_{20}$	I_h	320.15	0.33	−0.26	0.25	−0.01	−0.20	
$Li@C_{20}H_{20}$	I_h	50.61	0.52	−0.28	0.26	−0.02	−0.40	52.29
$Li^+@C_{20}H_{20}$	I_h	−12.70	0.90	−0.29	0.29	0.00	0.00	17.97
$Li^-@C_{20}H_{20}$	I_h	52.97	−0.04	−0.27	0.23	−0.04	−0.80	57.13
$Na@C_{20}H_{20}$	I_h	116.84	0.41	−0.28	0.26	−0.02	−0.40	118.36
$Na^+@C_{20}H_{20}$	I_h	55.33	0.88	−0.28	0.29	0.01	0.20	74.37
$Be@C_{20}H_{20}$	C_{5v}	127.70	1.25	−0.30[c]	0.24[c]	−0.06[c]	−1.20[c]	133.51
$Be^+@C_{20}H_{20}$	C_{5v}	−1.26	1.32	−0.30[c]	0.29[c]	−0.01[c]	−0.20[c]	57.82
$Be^{2+}@C_{20}H_{20}$	C_{5v}	−236.29	1.73	−0.32[c]	0.33[c]	0.01[c]	0.20[c]	16.46
$Mg@C_{20}H_{20}$	I_h	180.51	1.33	−0.31	0.24	−0.07	−1.40	187.27
$Mg^+@C_{20}H_{20}$	I_h	86.89	1.51	−0.31	0.28	−0.03	−0.60	111.90
$Mg^{2+}@C_{20}H_{20}$	I_h	−118.03	1.69	−0.32	0.33	0.01	0.20	11.79

[a] The inclusion energy was evaluated by comparing the ZPE corrected energy of the endohedral $X@C_{20}H_{20}$ complex with the sum of the individual components ZPE corrected energies. [b] Absolute exohedral complex energy subtracted from the absolute endohedral complex energy. See Table 6 for exohedral binding energies. [c] Average value obtained by summing the natural charge for all atoms (either C or H) and dividing by the total number of atoms.

TABLE 6: Exohedral C_{5v} $X-C_{20}H_{20}$ B3LYP/6-311+G(d,p) Absolute Energy (H_a), Exohedral Binding Energy (E_{bind}; kcal/mol), and B3LYP/6-311+G(d,p) Optimized Bond Lengths (Å) between X and the Cage (see Figure 9 for details)[c]

X	energy	ZPE	ω_1	E_{bind}	r_{C-C}	r_{C-H}	r_{C-X}	r_{H-X}
He	−777.27285			−0.12[a]	1.555	1.092	4.312	3.797
Ne	−903.32036			−0.21[a]	1.555	1.092	3.831	3.374
Li	−781.85103			−0.05[a]	1.555	1.092	5.073	4.491
Na	−936.64663			−0.14[a]	1.555	1.092	5.036	4.457
Be	−789.03097			−0.02[a]	1.555	1.092	8.057	7.354
Mg	−974.45278			−0.09[a]	1.555	1.092	5.665	5.048
Li^-	−781.87488			−2.14[a]	1.553	1.093	5.132	4.536
Li^+	−781.69502	226.65	170.9	−31.67[b]	1.570	1.100	2.223	2.237
Na^+	−936.47883	226.13	91.3	−19.84[b]	1.564	1.100	2.681	2.511
Be^+	−788.78683	226.55	178.0	−57.03[b]	1.590	1.097	1.969	2.139
Be^{2+}	−788.38735	226.73	436.2	−235.21[b]	1.656	1.099	1.730	2.126
Mg^+	−974.20763	225.72	65.1	−24.30[b]	1.565	1.102	2.617	2.473
Mg^{2+}	−973.80648	225.03	190.9	−129.17[b]	1.588	1.110	2.246	2.293

[a] Absolute energy of $C_{20}H_{20}$ plus X subtracted from the absolute exohedral complex energy. [b] ZPE corrected absolute energy of $C_{20}H_{20}$ plus X subtracted from the ZPE corrected absolute exohedral complex energy. [c] ZPE (kcal/mol) and fundamental vibrational frequencies (cm^{-1}) computed at B3LYP/6-31G(d) using geometries optimized at the same level.

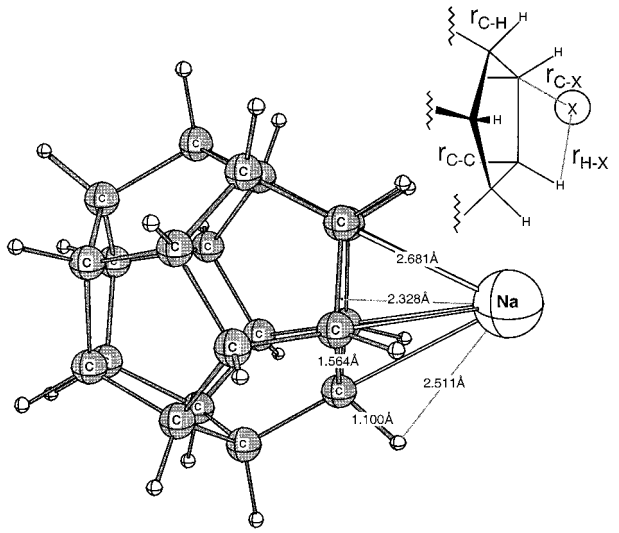

Figure 9. B3LYP/6-311+G(d,p) optimized $Na^+-C_{20}H_{20}$ exohedral complex.

changes in $He@C_{20}H_{20}$ and $Ne@C_{20}H_{20}$ geometries following introduction of He and Ne at MP2/6-311G(d,p).

$H@C_{20}H_{20}$ and $Li^+@C_{20}H_{20}$ were also optimized at B3LYP/6-31G(d) in C_{5v} symmetry, starting with X against an inner dodecahedrane face (cf. C_{5v} $Be^{2+}@C_{20}H_{20}$). The optimizations, however, revert to the I_h symmetric structures, with the endohedral species moving to the cage centers. It appears that Li^+ is not small enough to overcome the steric repulsion (crowding) from the cage in a C_{5v} face localized endohedral structure. A more interesting result is obtained when a hydrogen atom is placed on a C_3 axis, adjacent to a cage carbon and B3LYP/6-31G(d) optimized. The C_{3v} $C_{20}H_{21}$ structure shown in Figure 6 has an endohedral C−H bond and an exohedral coordinated hydrogen atom. This species is a UB3LYP/6-31G-(d) minimum (ω_1 = 638.3 cm^{-1}), 19.9 kcal/mol + ZPE less stable than I_h $H@C_{20}H_{20}$.

Table 6 summarizes select geometrical parameters (shown in Figure 9 inset) for optimized exohedral complexes, $X-C_{20}H_{20}$ (X = Li, Li^+, Li^-, Na, Na^+, Be, Be^+, and Be^{2+}). First, the C−X bond lengths for exohedral Be^+ (1.969 Å) and Be^{2+} (1.730 Å) are very similar to their endohedral distances of 1.758 and 1.735 Å, respectively, shown in Figure 5. This highlights the excellent fit that the cation and dication make to the internal cage face in the C_{5v} symmetric endohedral complexes. The Li, Li^-, Na, Be, and Mg C−X distances are all greater than 5 Å and these exohedral species are only weakly bound. Figure 10 shows a plot of the C−C bond length in the cage face adjacent to exohedral X for $X-C_{20}H_{20}$ (X = Li, Li^+, Li^-, Na, Na^+, Be, Be^+, and Be^{2+}); with the exception of Be^{2+}, the C−C bond lengths are essentially unchanged. The $Be^{2+}-C_{20}H_{20}$ C−C bonds are polarized by the adjacent tight fitting dication and the long bonds have increased p character (vide infra).

Inclusion Energies. Table 5 shows the ZPE corrected endohedral inclusion energies (E_{inc}) for $X@C_{20}H_{20}$ (H, He, Ne, Ar, Li, Li^+, Na, Na^+, Be, Be^+, Be^{2+}, Mg, Mg^+, and Mg^{2+}), evaluated by comparing the energy of the endohedral complex with the sum of X and dodecahedrane. E_{inc} is significantly exothermic for the dications Be^{2+} (−236.3 kcal/mol) and Mg^{2+} (−118.0 kcal/mol). In contrast, Li^+ is stable inside $C_{20}H_{20}$ by a

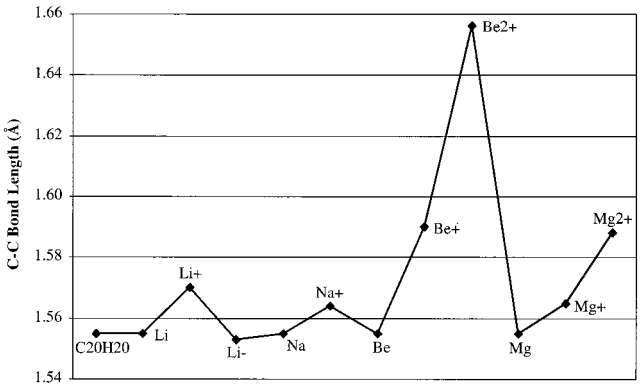

Figure 10. B3LYP/6-311+G(d,p) optimized C−C bond lengths in the dodecahedrane five-membered rings coordinated to exohedral metals, cations, and dications. This bond is labeled r_{C-C} in Figure 9.

mere 12.7 kcal/mol relative to separated Li^+ and dodecahedrane. Assuming Li^+ and Mg^{2+} have roughly equivalent radii, this result indicates that in the absence of size effects, E_{inc} is determined by the charge on X. However, the size of the encapsulated species is also very important, with Be^{2+} clearly more stable inside dodecahedrane than Mg^{2+} and Li^+ preferred over Na^+ by 68.0 kcal/mol.

The inclusion energies in Table 5 are in qualitative agreement with earlier low level estimates[13,14] and reproduce the recent B3LYP/6-311G(d,p) + ZPE endohedral inclusion energies of Jimenez-Vazquez et al.[15] However, the accord with their basis set superposition error (BSSE), counterpoise-corrected MP2/6-311G(d,p)//MP2/6-311G(d,p) + B3LYP/6-311G(d,p) ZPE + BSSE "best estimates" (Table 1) of 33.75 kcal/mol ($He@C_{20}H_{20}$) and 98.34 kcal/mol ($Ne@C_{20}H_{20}$) is less satisfactory. The greater than 4 kcal/mol discrepancies come from their non-ZPE corrected MP2 inclusion energies ($He@C_{20}H_{20}$ = 27.83 kcal/mol; $Ne@C_{20}H_{20}$ = 88.30 kcal/mol), which are significantly ($He@C_{20}H_{20}$ = 6.34 kcal/mol; $Ne@C_{20}H_{20}$ = 9.16 kcal/mol) lower than their non-ZPE corrected B3LYP/6-311G(d,p) stabilities ($He@C_{20}H_{20}$ = 34.17 kcal/mol; $Ne@C_{20}H_{20}$ = 97.46 kcal/mol). Their counterpoise-correction was 10% of the non-ZPE corrected MP2 inclusion energy (2.78 kcal/mol); however, typical of DFT,[39] the BSSE correction to the B3LYP/6-311G(d,p) energy (0.18 kcal/mol) was negligible. Therefore, in view of the large basis set superposition error and lengthy execution times associated with MP2 calculations, it appears that density functional theory is advantageous when computing supermolecular endohedral clusters.

Some interesting comparisons may be made between published fullerene inclusion energies and the dodecahedrane results. Our $X@C_{20}H_{20}$ (X = He, Ne, and Ar) inclusion energies (Table 5), are much larger than the $He@C_{60}$ (−0.3 kcal/mol), $Ne@C_{60}$ (−1.9 kcal/mol), and $Ar@C_{60}$ (−2.5 kcal/mol) counterpoise-corrected MP2/6-31G(d,p) inclusion energies of Bühl, Patchkovskii, and Thiel.[40] The differences in E_{inc} range from 38.2 kcal/mol for He through to 322.7 kcal/mol for Ar and highlights the 40% difference in interior diameter between the cages. Lithium cation, on the other hand appears to be only slightly less stable inside dodecahedrane than inside C_{60}. Varganov, Avramov, and Ovchinnikov[41] reported HF/3-21G $Li^+@C_{60}$ inclusion energies of −27.7 kcal/mol (T_h), −32.6 kcal/mol (C_{5v}), and −33.8 kcal/mol (C_{3v}) are in qualitative agreement with our B3LYP/6-311+G(d,p) $Li^+@C_{20}H_{20}$ (−12.7 kcal/mol) energy.

For dodecahedrane encapsulated metals, E_{inc} becomes more endothermic in the series Li, Na, Be, and Mg, following the increase in atomic radius along a period and down a group of the periodic table. The same trend was found by Sun, Wang, Yu, Ohno, and Kawazoe[42] who reported combined pseudopotential GGA DFT plane-wave basis inclusion energies of $Li@C_{32}$ (−53.1 kcal/mol), $Na@C_{32}$ (−26.9 kcal/mol), $K@C_{32}$ (13.7 kcal/mol), and $Be@C_{32}$ (6.9 kcal/mol). Interestingly, when the size of the two cages is compared, their E_{inc} results do not correspond with our dodecahedrane data. The average internal diameter of C_2 symmetric C_{32} is around 5.3 Å, about 1 Å wider than $C_{20}H_{20}$ (4.4 Å) and yet by their results Li, Na, and Be are >100 kcal/mol more stable encapsulated in C_{32}. The inclusion energies of Sun et al.[42] are corroborated in part by the HF/DZ inclusion energies of Guo, Smalley, and Scuseria[43] who report E_{inc} $Mg@C_{28}$ = −36.1 kcal/mol. T_d symmetric C_{28} (diameter 4.9 Å) is almost the same diameter as dodecahedrane. However, Mg is 200 kcal/mol more stable, relative to respective isolated components, when encapsulated by C_{28}. Clearly, improved binding is occurring between the metals and fullerene cages, which are much better able to encapsulate the metals than $C_{20}H_{20}$.

A salient alternative with which our endohedral inclusion energies may be compared is the corresponding exohedral binding energies (E_{bind} kcal/mol), shown in Table 6, which show a charge and size dependence much the same as E_{inc}. The small dication Be^{2+} has the most exothermic binding energy, followed by Mg^{2+} and then the cations Be^+, Li^+, Mg^+, and Na^+. Metals Li, Na, Mg, and Be have binding energies close to zero while Li^- binds $C_{20}H_{20}$ very weakly (−2.1 kcal/mol). The ZPE corrected energy difference between the exohedral and endohedral structures, termed the isomerization energy,[44] E_{isom} (kcal/mol) in Table 5, indicates that the exohedral species are in general energetically more favorable. E_{isom} is smallest when Mg^{2+} is the encapsulated species, with an isomerization energy of 11.8 kcal/mol, it is close to thermoneutral. The isomerization energies of Li^+ (18.0 kcal/mol) and Be^{2+} (16.5 kcal/mol) are also relatively low when compared, for example, with Mg (187.3 kcal/mol). While the endohedral structures are less favorable than the exohedral adducts, such unfavorable energetics are not prohibitive. For example, $He@C_{20}H_{20}$ was prepared[10] despite the He isomerization energy of 35.4 kcal/mol.

Natural Charge and Bond Order Analyses. The natural charges, listed in Table 5, provide interesting insights into the distribution of charge within the endohedral complexes. The +0.52 lithium charge in $Li@C_{20}H_{20}$ exemplifies the significant positive charges of encapsulated metal atoms. The most ionized encapsulated metal atom in Table 5 is magnesium (+1.33); hence, it is expected to have the greatest electron delocalization into the C−H antibonding $C_{20}H_{20}$ LUMO (see Figure 2). Indeed, $Mg@C_{20}H_{20}$ has the longest C−H bond length (1.098 Å) of the metal dodecahedrane derivatives in Table 3. Furthermore, the natural charges help explain why beryllium metal is C_{5v} localized in $Be@C_{20}H_{20}$, with a charge on the encapsulated beryllium metal of +1.25. In this oxidized state it too is small to fit into the cage center, preferring a C_{5v} face localized structure that maximizes the electrostatic interaction. Be^{2+} (charge +1.73) behaves similarly.

Dodecahedrane encapsulated H, He, and Ne are essentially neutral and, consistent with Disch and Schulman's[14] earlier findings for $He@C_{20}H_{20}$, there is no charge transfer to the cage. The charge on encapsulated Ar is +0.33, reflecting the lower electronegativity[45] of this tight-fitting noble gas nucleus compared with helium or neon.

Generally, the hydrogen charges of cation and dication derivatives are more positive than their neutral counterparts, consistent with C^--H^+ bond polarization and the trend of $X@C_{20}H_{20}^{]+,2+}$ cations and dications to have shorter C−H bonds

TABLE 7: B3LYP/6-311+G(d,p) Vertical and Adiabatic IP (kcal/mol), B3LYP/6-311+G(d,p), and Experimental Gas Phase IP of Free Atoms and IP Reductions Due to Encapsulation, i.e., Computed Atomic IP − Adiabatic X@$C_{20}H_{20}$ IP (kcal/mol) (Values also shown in eV in parentheses)

ionization process	adiabatic IP	vertical IP	expt IP	IP reduction
$Li^- \rightarrow Li + e^-$	12.87 (0.56)	−	−	−
$Li^-@C_{20}H_{20} \rightarrow Li@C_{20}H_{20} + e^-$ (I_h)	10.12 (0.44)	10.14 (0.44)	−	2.75 (0.12)
$Li \rightarrow Li^+ + e^-$	129.53 (5.61)	−	124.35[60] (5.39)	−
$Li@C_{20}H_{20} \rightarrow Li^+@C_{20}H_{20} + e^-$ (I_h)	63.63 (2.76)	63.89 (2.77)	−	65.90 (2.86)
$Na \rightarrow Na^+ + e^-$	125.01 (5.42)	−	118.58[61] (5.14)	−
$Na@C_{20}H_{20} \rightarrow Na^+@C_{20}H_{20} + e^-$($I_h$)	61.31 (2.66)	61.50 (2.67)	−	63.69 (2.76)
$Be \rightarrow Be^+ + e^-$	210.22 (9.11)	−	215.01[62] (9.32)	−
$Be@C_{20}H_{20} \rightarrow Be^+@C_{20}H_{20} + e^-$ (C_{5v})	84.54 (3.66)	86.09 (3.73)	−	125.67 (5.45)
$Be^+ \rightarrow Be^{2+} + e^-$	428.86 (18.59)	−	−	−
$Be^+@C_{20}H_{20} \rightarrow Be^{2+}@C_{20}H_{20} + e^-$ (C_{5v})	193.14 (8.37)	193.62 (8.39)	−	235.72 (10.22)
$Mg \rightarrow Mg^+ + e^-$	178.21 (7.72)	−	176.49[63] (7.65)	−
$Mg@C_{20}H_{20} \rightarrow Mg^+@C_{20}H_{20} + e^-$ (I_h)	78.46 (3.40)	79.15 (3.43)	−	99.75 (4.32)
$Mg^+ \rightarrow Mg^{2+} + e^-$	356.59 (15.46)	−	−	−
$Mg^+@C_{20}H_{20} \rightarrow Mg^{2+}@C_{20}H_{20} + e^-$ (I_h)	151.63 (6.57)	152.15 (6.60)	−	204.96 (8.88)

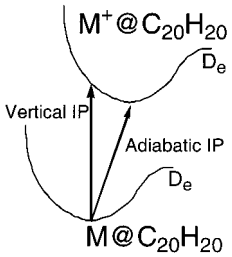

Figure 11. Schematic showing vertical and adiabatic ionization processes.

relative to their neutral derivatives (vide infra). Shorter C−H bond lengths imply increased s character. This is exactly what is seen in the NBO computed bond hybridizations, for example, C−C $sp^{2.98}$ and C−H $sp^{3.09}$ in $Li@C_{20}H_{20}$ compared with C−C $sp^{3.09}$ and C−H $sp^{2.79}$ in $Li^+@C_{20}H_{20}$. An additional comparison is the bond hybridizations for $Mg@C_{20}H_{20}$ (C−C $sp^{3.06}$; C−H $sp^{2.88}$), for $Mg^+@C_{20}H_{20}$ (C−C $sp^{3.10}$; C−H $sp^{2.76}$), and for $Mg^{2+}@C_{20}H_{20}$ (C−C $sp^{3.20}$; C−H $sp^{2.54}$). Increased p character in the C−C bond framework also is obvious, consistent with the slight cage expansion we observe when comparing neutral $X@C_{20}H_{20}$ (X = Li, Na, and Mg) with $X@C_{20}H_{20}^{1+,\,2+}$ cation and dication geometries.

Ionization Potentials. Vertical and adiabatic ionization potentials (IP; Figure 11) for $X@C_{20}H_{20}$ (X = Li^-, Li, Na, Be, Be^+, Mg, and Mg^+) endohedral derivatives are summarized in Table 7. Adiabatic electron affinities computed using the B3LYP functional and triple-ζ quality basis sets reproduce experimental values consistently.[46,47] Compared with the experimental ionization potentials, our $M \rightarrow M^+ + e^-$ adiabatic IPs have a median error of ±5.0 kcal/mol.

The IPs of encapsulated Li, Na, Be, and Mg are reduced considerably relative to the free metal. Significantly less than the ionization potential reductions of either Li, Na, and Mg, the 235.7 kcal/mol (10.2 eV) reduction in C_{5v} Be^+ IP ($Be^+@C_{20}H_{20} \rightarrow Be^{2+}@C_{20}H_{20} + e^-$) is most dramatic, in part reflecting the radius of the Be^{2+} dication. The C_{5v} Be IP ($Be@C_{20}H_{20} \rightarrow Be^+@C_{20}H_{20} + e^-$) and I_h Mg^+ IP ($Mg^+@C_{20}H_{20} \rightarrow Mg^{2+}@C_{20}H_{20} + e^-$) reductions of 125.7 kcal/mol (5.5 eV) and 205.0 kcal/mol (8.9 eV), respectively, also are considerable. Boldyrev and co-workers[48−50] defined species with first ionization potentials less than the Cs atom (90.0 kcal/mol; 3.9 eV) as "superalkalis". Ranging from 61.5 kcal/mol (2.7 eV) to 86.1 kcal/mol (3.7 eV), the first ionization potentials for encapsulated Li, Na, Be, and Mg are significantly less than cesium, i.e., $M@C_{20}H_{20}$ (M = Li, Na, Be, and Mg) are superalkalis.

TABLE 8: B3LYP/6-311+G(d,p) Isotropic Magnetic Shielding Tensor and Chemical Shift (δ) for Nuclei in Dodecahedrane and Endohedral Dodecahedrane Complexes[a]

	carbon (δ)[b]	hydrogen (δ)[b]	X (δ)[c]
$Bq@C_{20}H_{20}$ (I_h)	110.2 (73.8)	28.5 (3.5)	−0.4 (0.4)
Bq ring center			2.2 (−2.2)
Bq 1.0 Å above ring center			1.9 (−1.9)
$He@C_{20}H_{20}$ (I_h)	107.0 (77.0)	28.5 (3.5)	59.0 (0.9)
[B3LYP/6-311+G(3df,2p)]	[106.5 (77.5)]	[28.2 (3.8)]	[58.6 (1.3)]
Jimenez-Vazquez et al.[15,d]			59.9 (1.51)
$Li^+@C_{20}H_{20}$ (I_h)	111.3 (72.7)	27.8 (4.2)	93.4 (1.9)

[a] Note that in the case of dodecahedrane a ghost atom (Bq) was placed at the cage center, the center of a five-membered ring face, and 1 Å above a five-membered ring face. B3LYP/6-311+G(3df,2p) data reported in brackets. [b] Obtained by subtracting the absolute isotropic shielding from that of TMS (C = 184.0 ppm [183.0 ppm]; H = 32.0 ppm [31.7 ppm]). [c] Obtained by subtracting the absolute isotropic shielding of encapsulated X from the unencapsulated atom (He = 59.9 ppm [59.9 ppm]; Li^+ = 95.3 ppm). Following the NICS convention the sign of the Bq shielding tensor was inverted. [d] B3LYP/6-311+G(3df,2p)//MP2/6-311G(d,p). Isotropic shielding of encapsulated He 58.4 ppm.

Comparable reductions in endohedral fullerene complex ionization potentials have not been reported. For example, neither the endohedral HF/DZ $M@C_{28}$ (M = Mg, Ca, Al, Sc, S, Si, Ge, Sn, Ti, and Zr) ionization potentials predicted by Guo et al.[43] nor the LSDA/DNP $M@C_{60}$ (M = Li, Na, K, Be, Mg, Ca, B, Al, and La) ionization potentials predicted by Broclawik and Eilmes[51] show an appreciable IP reduction due to encapsulation seen here for $X@C_{20}H_{20}$. However, they did not employ theoretical levels that include the electron correlation effects, important for describing the interaction between fullerenes and noble gases[52] and possibly closed shell metal−cage interactions.

NMR Chemical Shifts. Table 8 summarizes the $C_{20}H_{20}$ NICS and $X@C_{20}H_{20}$ (X = He and Li^+) NMR chemical shifts (referenced against TMS and unencapsulated X). The endohedral He (δ = 0.9 ppm) and Li^+ (δ = 1.9 ppm) are slightly deshielded by the cage, in contrast with experimental ^{3}He NMR shifts for $He@C_{60}$ (I_h; −6.3 ppm),[5] $He@C_{70}$ (D_{5h}; −28.8 ppm),[5] and $He@C_{60}H_{36}$ (D_{3d}; −7.7 ppm). An encapsulated helium nucleus acts as probe of the magnetic environment within its cage host,[53,54] as does a NICS point (Bq) at the cage center ($Bq@C_{20}H_{20}$) and there is strong accord between endohedral He (0.4 ppm) and Bq (0.9 ppm) chemical shifts. $C_{20}H_{20}$ lacks a fullerene-type mobile π electron system and, not surprisingly, $He@C_{20}H_{20}$ does not experience the upfield ring current induced endohedral He chemical shift observed for the fullerene complexes.

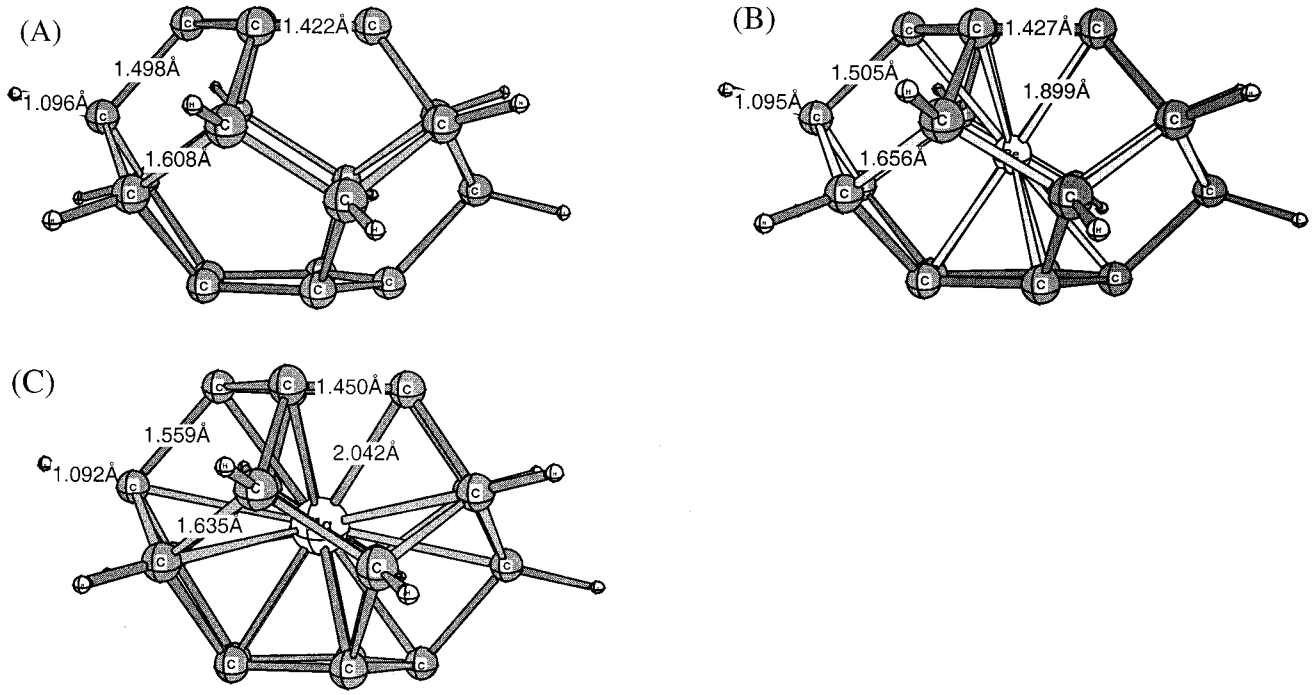

Figure 12. B3LYP/6-31G(d) optimized D_{5d} $C_{20}H_{10}$ (A), $Be@C_{20}H_{10}$ (B), and $Mg@C_{20}H_{10}$ (C).

The $He@C_{20}H_{20}$ NMR chemical shift was re-computed using GIAO/B3LYP/6-311+G(3df,2p) to enable comparison with the results of Jimenez-Vazquez et al.[15] ($\delta = 1.5$ ppm).[14] At this level our helium chemical shift is $\delta = 1.3$ ppm, 0.4 ppm further downfield than at GIAO/B3LYP/6-311+G(d,p) and in close agreement with Jimenez-Vazquez et al.[15]

NICS at the center of a $C_{20}H_{20}$ cage face is -2.2 ppm and, compared with NICS at the center of benzene (-11.5 ppm) or cyclohexane (-2.1 ppm),[55] indicates a lack of cyclic electron delocalization in the five-membered ring. Dissected NICS[31,32] show that dodecahedrane C−C and C−H σ bonds contribute around 6 ppm and -4 ppm, respectively, to NICS at the cage center and that the small deshielding of encapsulated helium arises due to the C−C σ framework of dodecahedrane. The C−C and C−H bond contributions to NICS at the center of a dodecahedrane cage face are 5.8 ppm and -7.6 ppm, respectively, and in this case, the local effect of the five adjacent C−H bonds overwhelms the deshielding C−C σ bonds.

Overall the effect of encapsulation on the NMR spectra of dodecahedrane is minimal. The ^{13}C $He@C_{20}H_{20}$ and $Li^+@C_{20}H_{20}$ chemical shifts are shifted relative to dodecahedrane by a mere 3.2 and 1.1 ppm, respectively. The ^1H $Li^+@C_{20}H_{20}$ chemical shift is displaced by 0.7 ppm relative to dodecahedrane while the protons in $He@C_{20}H_{20}$ have the same chemical shift as the free cage. It appears, therefore, that while ^1H NMR may be useful for detecting metal cation complexes such as $Li^+@C_{20}H_{20}$, ^{13}C NMR chemical shifts for $C_{20}H_{20}$ and $X@C_{20}H_{20}$ are too close to differentiate.

Caged Beryllocene ($Be@C_{20}H_{10}$) and Magnesocene ($Mg@C_{20}H_{10}$). The E_{inc} values shown in Table 5 become more endothermic in the series $Li@C_{20}H_{20}$ (50.6 kcal/mol), $Na@C_{20}H_{20}$ (116.8 kcal/mol), $Be@C_{20}H_{20}$ (127.7 kcal/mol), and $Mg@C_{20}H_{20}$ (180.5 kcal/mol), following the increase in atomic radius along a period and down a group of the periodic table. These inclusion energies reflect the unfavorable formation of the endohedral metal complexes, which is also indicated in their thermoneutral $M-C_{20}H_{20}$ (M = Li, Na, Be, and Mg) exohedral binding energies shown in Table 6. Removal of 10 dodecahedrane hydrogens from opposite cage faces can result in strong metallocene-type bonding[56] involving some endohedral metals. This strategy should improve $M@C_{20}H_{10}$ complex stabilities. The $Be@C_{20}H_{10}$ beryllocene sandwich complex shown in Figure 12 is 75.3 kcal/mol (Table 9) more stable than its isolated components, considerably better than the $Be@C_{20}H_{20}$ inclusion energy. Similarly, the 35.9 kcal/mol magnesocene ($Mg@C_{20}H_{10}$; Figure 12) inclusion energy is over 140 kcal/mol less endothermic than $Mg@C_{20}H_{20}$.

TABLE 9: Endohedral D_{5d} $M-C_{20}H_{20}$ (M = Be, Mg; see Figure 12) B3LYP/6-311+G(d,p) Absolute Energies and Inclusion Energies (E_{Inc}; kcal/mol).[a] ZPE (kcal/mol), Fundamental Vibrational Frequencies (cm^{-1}) and Natural Charges Computed at B3LYP/6-31G(d) Using Geometries Optimized at the Same Level

M	energy	ZPE	ω_1	E_{inc}[a]	q_X	q_C	q_C[b]	q_H
c	−767.79389	149.26	410.4			−0.01	−0.25	0.26
Be	−782.75190	149.60	444.5	−75.27	1.40	−0.16	−0.24	0.26
Mg	−967.98279	147.83	316.0	35.92	1.64	−0.15	−0.29	0.27

[a] The inclusion energy was evaluated by comparing the ZPE corrected energy of the endohedral $X@C_{20}H_{10}$ complex with the sum of the individual components ZPE corrected energies. [b] Carbon atoms with hydrogens attached. [c] $C_{20}H_{10}$ (D_{5d}) minimum is a triplet state.

The experimental structure of beryllocene $(C_5H_5)_2Be$ is a slipped sandwich, with a $\eta^1-\eta^5$ coordinated (C_s) conformation,[57] that results from unfavorable interactions between the adjacent cyclopentadienyl (CPD) units.[56,58,59] CPD ring slippage in our $Be@C_{20}H_{10}$, however, does not occur because of the incarcerating −CH− groups that make up the cage. Compared with the structure of $Mg@C_{20}H_{10}$, the cage in $Be@C_{20}H_{10}$ is somewhat flattened with the metal capping cyclopentyl rings closer together (C−Be = 1.899 Å) and expanded equatorial C−C bonds (cf. (Mg)C−C = 1.635 Å and (Be)C−C = 1.656 Å). In $Be@C_{20}H_{10}$ the magnesocene structure is more nearly spherical, with magnesium interactions with both the polar (2.042 Å) and equatorial (2.281 Å) carbons. The endohedral Mg, but not the endohedral Be, contacts all twenty cage carbon atoms and this difference in structure is reflected in the natural charges on beryllium (+1.40) and magnesium (+1.64), with the polar carbons sharing the negative charge in both cases.

Conclusions

$X@C_{20}H_{20}$ (X = H, He, Ne, Ar, Li, Li^+, Na, Na^+, Mg, Mg^+, and Mg^{2+}) derivatives have B3LYP/6-311G(d,p) I_h minima whereas $Be@C_{20}H_{20}$, $Be^+@C_{20}H_{20}$, and $Be^{2+}@C_{20}H_{20}$ favor face-localized C_{5v} symmetry. Endohedral hydrogen and noble gas atoms (He, Ne, and Ar) stretch the cage roughly in proportion to their radii, expanding the dodecahedrane C−C bond lengths from 1.562 Å ($H@C_{20}H_{20}$) to 1.623 Å ($Ar@C_{20}H_{20}$). However, the trend is somewhat different and the cage is slightly more compact when encapsulating a metal atom as compared with its corresponding cation or dication. For example, dodecahedrane C−C bond lengths increase in the series: $Mg^{2+}@C_{20}H_{20}$ (1.589 Å) > $Mg^+@C_{20}H_{20}$ (1.587 Å) > $Mg@C_{20}H_{20}$ (1.585 Å). This is due to donation of electron density from the encapsulated metal atom into the C−C bonding and C−H antibonding endohedral complex HOMO, which has a structure closely resembling the LUMO (A_{1g}) of dodecahedrane.

The ZPE corrected inclusion energies of $Li^+@C_{20}H_{20}$ (I_h; −12.7 kcal/mol), $Be^+@C_{20}H_{20}$ (C_{5v}; −1.3 kcal/mol), $Be^{2+}@C_{20}H_{20}$ (C_{5v}; −236.3 kcal/mol), and $Mg^{2+}@C_{20}H_{20}$ (I_h; −118.0 kcal/mol) are exothermic compared with their isolated components, due to polarization stabilization of these charged complexes. However, all the endohedral dodecahedrane complexes are higher in energy than their corresponding exohedral isomers, i.e., exohedral binding is favored over endohedral encapsulation. Our $X@C_{20}H_{20}$ (X = He and Ne) inclusion energies are in agreement with recently reported B3LYP/6-311G(d,p) energies.[15] Endohedral metal atoms are stabilized by forming metallocene structures such as $Be@C_{20}H_{10}$ (D_{5d}), which is 75.3 kcal/mol more stable than its isolated components, in contrast to the large, 127.7 kcal/mol endothermic inclusion energy of $Be@C_{20}H_{20}$ (I_h).

The reductions in ionization potentials of metal atoms when dodecahedrane encapsulated are remarkable. For example, the B3LYP/6-311+G(d,p) adiabatic IP of $Li@C_{20}H_{20} \rightarrow Li^+@C_{20}H_{20} + e^-$ is 63.6 kcal/mol (2.8 eV) versus the Li atom IP of 129.5 kcal/mol (5.6 eV). $M@C_{20}H_{20}$ (M = Li, Na, Be, and Mg) have smaller first ionization potentials than the IP of Cs (90.0 kcal/mol; 3.9 eV) and thus are "superalkalis".[48−50]

Endohedral He (0.9 ppm, B3LYP/6-311+G(3df,2p) 1.3 ppm) and Li^+ (1.9 ppm) nuclei were deshielded slightly by the C−C σ bonds of the cage. NICS computed at the center of dodecahedrane (0.4 ppm) and a five-membered ring face (−2.2 ppm) are normal and show no evidence for any unusual ring or cage electron delocalization effects.

Acknowledgment. We thank Dr. Kai Exner, Prof. Peter Schreiner, Prof. Hugo Jimenez-Vazquez, and Prof. Martin Saunders for fruitful discussions.

Note Added in Proof. $H@C_{20}H_{20}$ is much less stable than an isomer with a CH_2 group and a ruptured C−C bond. This and the preferences of additional endohedral atom complexes for skeletal positions will be reported shortly (Chen, Z.; Jiao, H.; Moran, D.; Hirsch, A.; Thiel, W.; Schleyer, P. v. R.; manuscript in preparation).

References and Notes

(1) Heath, J. R.; O'Brien, S. C.; Zhang, Q.; Liu, Y.; Curl, R. F.; Kroto, H. W.; Smalley, R. E. *J. Am. Chem. Soc.* **1985**, *107*, 7779.

(2) Stevenson, S.; Burbank, P.; Harich, K.; Sun, Z.; Dorn, H. C.; Loosdrecht, P. H. M. v.; deVries, M. S.; Salem, J. R.; Kiang, C.-H.; Johnson, R. D.; Bethune, D. S. *J. Phys. Chem. A* **1998**, *102*, 2833.

(3) Laskin, J.; Peres, T.; Khong, A.; Jimenez-Vazquez, H. A.; Cross, R. J.; Saunders, M.; Bethune, D. S.; de Vries, M. S.; Lifshitz, C. *Int. J. Mass Spectrom.* **1999**, *185/186/187*, 61.

(4) Hirsch, A. *Angew. Chem., Int Ed. Engl.* **2001**, *40*, 1195.

(5) Saunders, M.; Jimenez-Vazquez, H. A.; Cross, R. J.; Mroczkowski, S.; Freedberg, D. I.; Anet, A. L. *Nature* **1994**, *367*, 256.

(6) Saunders, M.; Jimenez-Vazquez, H. A.; Cross, R. J.; Mroczkowski, S.; Gross, M. L.; Giblin, D. E.; Poreda, R. J. *J. Am. Chem. Soc.* **1994**, *116*, 2193.

(7) Peres, T.; Cao, B. P.; Cui, W. D.; Khong, A.; Cross, R. J.; Saunders: M.; Lifshitz, C. *Int. J. Mass Spectrom.* **2001**, *210*, 241.

(8) Mauser, H.; van eikema Hommes, N. J. R.; Clark, T.; Hirsch, A.; Pietzak, B.; Wedinger, A.; Dunsch, L. *Angew. Chem., Int Ed. Engl.* **1997**, *36*, 2835.

(9) Shimshi, R.; Cross, R. J.; Saunders, M. *J. Am. Chem. Soc.* **1997**, *119*, 1163.

(10) Cross, R. J.; Saunders, M.; Prinzbach, H. *Org. Lett.* **1999**, *1*, 1479.

(11) Schulman, J. M.; Disch, R. L. *J. Am. Chem. Soc.* **1978**, *100*, 5677.

(12) The "@" symbol indicates endohedral encapsulation of X while "−" implies exohedral coordination. While this symbolism is not necessarily correct chemically (e.g., NBO analysis shows $Li^-@C_{20}H_{20}$ should be written $Li@C_{20}H_{20}^-$), it is useful nevertheless.

(13) Dixon, D. A.; Deerfield, D.; Graham, G. D. *Chem. Phys. Lett.* **1981**, *78*, 161.

(14) Disch, R. L.; Schulman, J. M. *J. Am. Chem. Soc.* **1981**, *103*, 3297.

(15) Jimenez-Vazquez, H. A.; Tamariz, J.; Cross, R. J. *J. Phys. Chem. A* **2001**, *105*, 1315.

(16) Although the ^{3}He shift reported for $He@C_{20}H_{20}$ was correct, there were two errors in *J. Phys. Chem. A* **2001**, *105*, 1315 which fortuitously canceled. The authors agree. First, the value of the $He@C_{20}H_{20}$ He isotropic magnetic tensor should have been subtracted from He. Second, the encapsulated and free He shieldings were interchanged.

(17) Schleyer, P. v. R.; Najafian, K.; Mebel, A. *Inorg. Chem.* **1998**, *37*, 6765.

(18) Jemmis, E. D.; Balakrishnarajan, M. M. *J. Am. Chem Soc.* **2000**, *122*, 7392.

(19) Charkin, O. P.; Klimenko, N. M.; Moran, D.; Mebel, A. M.; Charkin, D. O.; Schleyer, P. v. R. *Inorg. Chem.*, submitted.

(20) Charkin, O. P.; Klimenko, N. M.; Moran, D.; Mebel, A. M.; Charkin, D. O.; Schleyer, P. v. R. *Inorg. Chem.* **2001**, *ASAP*.

(21) Charkin, O. P.; Klimenko, N. M.; Moran, D.; Mebel, A. M.; Schleyer, P. v. R. *Russ. J. Inorg. Chem.* **2001**, *46*, 110−120.

(22) Frisch, M. J.; Trucks, G. W.; Schlegel, H. B.; Scuseria, G. E.; Robb, M. A.; Cheeseman, J. R.; Zakrzewski, V. G.; Montgomery, J. A. J.; Stratmann, R. E.; Burant, J. C.; Dapprich, S.; Millam, J. M.; Daniels, A. D.; Kudin, K. N.; Strain, M. C.; Farkas, O.; Tomasi, J.; Barone, V.; Cossi, M.; Cammi, R.; Mennucci, B.; Pomelli, C.; Adamo, C.; Clifford, S.; Ochterski, J.; Petersson, G. A.; Ayala, P. Y.; Cui, Q.; Morokuma, K.; Malick, D. K.; Rabuck, A. D.; Raghavachari, K.; Foresman, J. B.; Cioslowski, J.; Ortiz, J. V.; Stefanov, B. B.; Liu, G.; Liashenko, A.; Piskorz, P.; Komaromi, I.; Gomperts, R.; Martin, R. L.; Fox, D. J.; Keith, T.; Al-Laham, M. A.; Peng, C. Y.; Nanayakkara, A.; Gonzalez, C.; Challacombe, M.; Gill, P. M. W.; Johnson, B.; Chen, W.; Wong, M. W.; Andres, J. L.; Gonzalez, C.; Head-Gordon, M.; Replogle, E. S.; Pople, J. A. Gaussian 98, revision A.7; Gaussian, Inc.: Pittsburgh, PA, 1998.

(23) Likewise, EPR ^{13}C and ^{1}H hyperfine splitting might be useful probes for odd-electron endohedral derivatives.

(24) Patchkovskii, S.; Thiel, W. *J. Chem. Phys.* **1997**, *106*, 1796.

(25) Ahlrichs, R.; Bar, M.; Haser, M.; Horn, H.; Kolmel, C. *Chem. Phys. Lett.* **1989**, *162*, 165.

(26) Treutler, O.; Ahlrichs, R. *J. Chem. Phys.* **1995**, *102*, 346.

(27) Frisch, M. J.; Trucks, G. W.; Schlegel, H. B.; Gill, P. M. W.; Johnson, B. G.; Robb, M. A.; Cheeseman, J. R.; Keith, T.; Petersson, G. A.; Montgomery, J. A.; Raghavachari, K.; Al-Laham, M. A.; Zakrzewski, V. G.; Ortiz, J. V.; Foresman, J. B.; Cioslowski, J.; Stefanov, B. B.; Nanayakkara, A.; Challacombe, M.; Peng, C. Y.; Ayala, P. Y.; Chen, W.; Wong, M. W.; Andres, J. L.; Replogle, E. S.; Gomperts, R.; Martin, R. L.; Fox, D. J.; Binkley, J. S.; DeFrees, D. J.; Baker, J.; Stewart, J. P.; Head-Gordon, M.; Gonzales, C.; Pople, J. A. Gaussian 94, revision E.2; Gaussian, Inc: Pittsburgh, PA, 1994.

(28) Frisch, A.; Frisch, M. J. *Gaussian 98 User's Reference*, 2nd ed.; Gaussian, Inc.: Pittsburgh, PA, 1999.

(29) Hehre, W. J.; Radom, L.; Pople, J. A.; Schleyer, P. v. R. *Ab Initio Molecular Orbital Theory*; John Wiley & Sons: New York, 1986.

(30) Glendening, E. D.; Reed, A. E.; Carpenter, J. E.; Weinhold, F. NBO Version 3.1; University of Wisconsin: Madison, 1996.

(31) Schleyer, P. v. R.; Maerker, C.; Dransfeld, A.; Jiao, H.; van Eikema Hommes, N. J. R. *J. Am. Chem. Soc.* **1996**, *118*, 6317.

(32) Schleyer, P. v. R.; Manoharan, M.; Wang, Z.-X.; Kiran, B.; Jiao, H.; Puchta, R.; Hommes, N. J. R. v. E. *Org. Lett.* **2001**, *3*, 2465.

(33) A Bq is a point in space with neither nuclear charge nor basis functions.

(34) Fleischer, U.; Kutzelnigg, W.; Lazzeretti, P.; Muhlenkamp, V. *J. Am. Chem. Soc.* **1994**, *116*, 5298.

(35) Malkin, V. G.; Malkina, O. L.; Eriksson, L. A.; Salahub, D. R. *J. Am. Chem. Soc.* **1994**, *116*, 5898.

(36) The absolute energy of dodecahedrane, dodecahedrane radical cation, and dodecahedrane radical anion are shown in Table 3. The equilibrium geometries of the dodecahedrane radical anion and radical cation are 9.68 kcal/mol + ZPE and 191.38 kcal/mol + ZPE less stable than dodecahedrane, respectively. The adiabatic electron affinity (EA) of dodecahedrane is endothermic by 9.68 kcal/mol—electrons generally do not bind exothermically to saturated hydrocarbons because the virtual molecular orbitals are too high in energy (Salzner, U.; Schleyer, P. v. R. *Chem. Phys. Lett.* **1992**, *199*, 267).

(37) Mauksch, M.; Schleyer, P. v. R. *Inorg. Chem.* **2001**, *40*, 1756−1769.

(38) That is, the cage expands when a cation or dication is encapsulated.

(39) Koch, W.; Holthausen, M. C. *A Chemist's Guide to Density Functional Theory*; Wiley-VCH: Weinheim, 2000.

(40) Buhl, M.; Patchkovskii, S.; Thiel, W. *Chem. Phys. Lett.* **1997**, *275*, 14.

(41) Varganov, S. A.; Avramov, P. V.; Ovchinnikov, S. G. *Phys. Solid State* **2000**, *42*, 378.

(42) Sun, Q.; Wang, Q.; Yu, J. Z.; Ohno, K.; Kawazoe, Y. *J. Phys.: Condens. Matter* **2001**, *13*, 1931.

(43) Guo, T.; Smalley, R. E.; Scuseria, G. E. *J. Chem. Phys.* **1993**, *99*, 352−359.

(44) Jemmis, E. D.; Balakrishnarajan, M. M. *J. Am. Chem Soc*. **2000**, *122*, 7392 referred to this quantity as the "strain energy".

(45) Huheey, J. E.; Keiter, E. A.; Keiter, R. L. *Inorganic Chemistry: Principles of Structure and Reactivity*, 4th ed.; Harper Collins: New York, 1993.

(46) Wesolowski, S. S.; Leininger, M. L.; Pentchev, P. N.; Schaefer, H. F., III. *J. Am. Chem Soc.* **2001**, *123*, 4023.

(47) Gonzales, J. M.; King, R. A.; Schaefer, H. F., III. *J. Chem. Phys.* **2000**, *113*, 567.

(48) Gutsev, G. L.; Boldyrev, A. I. *Adv. Chem. Phys.* **1985**, *51*, 169.

(49) Gutsev, G. L.; Boldyrev, A. I. *Chem. Phys. Lett.* **1982**, *92*, 262.

(50) Rehm, E.; Boldyrev, A. I.; Schleyer, P. v. R. *Inorg. Chem.* **1992**, *31*, 4834.

(51) Broclawik, E.; Eilmes, A. *J. Chem. Phys.* **1998**, *108*, 3498.

(52) Klopper, W.; Luthi, H. P.; Brupbacher, T.; Bauder, A. *J. Chem. Phys.* **1994**, *101*, 9747.

(53) Buhl, M. *Chem. Eur. J.* **1998**, *4*, 734.

(54) Buhl, M.; Thiel, W.; Jiao, H. J.; Schleyer, P. v. R.; Saunders, M.; Anet, F. A. L. *J. Am. Chem. Soc.* **1994**, *116*, 6005.

(55) Jiao, H.; Nagelkerke, R.; Kurtz, H. A.; Williams, R. V.; Borden, W. T.; Schleyer, P. v. R. *J. Am. Chem. Soc.* **1997**, *119*, 5921−5929.

(56) Sapunov, V. N.; Kirchner, K.; Schmid, R. *Coord. Chem. Rev.* **2001**, *214*, 143.

(57) Chiu, N.-S.; Schaefer, F. *J. Am. Chem. Soc.* **1978**, *100*, 2604.

(58) Cotton, F. A.; Wilkinson, G.; Murillo, C. A. *Advanced Inorganic Chemistry*, sixth ed.; John Willey and Sons: New York, 1999.

(59) Collins, J. B.; Schleyer, P. v. R. *Inorg. Chem.* **1977**, *16*, 152.

(60) Lorenzen, C. J.; Niemax, K. *J. Phys. B* **1982**, *15*, L139−L145.

(61) Ciocca, M.; Burkhardt, C. E.; Leventhal, J. J.; Bergeman, T. *Phys. Rev. A* **1992**, *45*, 4720.

(62) Beigang, R.; Schmidt, D.; West, P. J. *J. Phys. (Paris)* **1983**, *44*, 229.

(63) Kaufman, V.; Martin, W. C. *J. Phys. Chem. Ref. Data* **1991**, *20*, 83.